Supporting Information

Peisley et al. 10.1073/pnas.1208618109

SI Materials and Methods

Material Preparation. MDA5 and RIG-I were prepared as previously described (1). The caspase activation recruitment domain (CARD)-deletion MDA5 mutant MDA5h (287–1,025 amino acids) and its N-terminal SNAP (New England BioLabs) fusion construct ($MDA5h^{SNAP}$) were expressed from pET50b and purified using a combination of Ni-NTA and heparin affinity chromatography and size-exclusion chromatography (SEC) as for MDA5 and RIG-I (Fig. S1) (1). Purified protein was stored at −20 °C in the storage buffer consisting of 20 mM Hepes (pH 7.5), 150 mM NaCl, 5 mM DTT, and 50% (vol/vol) glycerol. For N-terminal fluorescent labeling of MDA5, RIG-I, and MDA5h, the proteins (~5 mg/mL) were incubated with 0.5 mM peptide (LPETGG) conjugated with HiL Hylite 647 or fluorescein (Anaspec) and 0.3 mM *Staphylococcus aureus* sortase A (a gift from Hidde Ploegh, Massachusetts Institute of Technology, Cambridge, MA) (2) at room temperature for 4–6 h. $MDA5h^{SNAP}$ was labeled with Alexa 647 benzylguanine (New England BioLabs) according to the manufacturer's instructions. Labeled protein was purified further by SEC to remove unincorporated dye and was stored in the storage buffer. Labeled proteins retain dsRNA-dependent ATP hydrolysis activity similar to that of unlabeled proteins (1).

RNAs (Table S1) were prepared by in vitro transcription using T7 RNA polymerase as described by Sherlin et al., *RNA,* 2001. The two complementary strands were cotranscribed, and the duplex was separated from unannealed single-stranded RNAs (ssRNAs) by 10% (wt/vol) acrylamide/ Tris/borate/EDTA (TBE) (15–20 bp), 8.5% (wt/vol) acrylamide/TBE (62–162 bp), or 1% (wt/vol) agarose/Tris/acetate/EDTA (512–2,012 bp) gel electrophoresis. RNA was gel-extracted by electroelution using Elutrap (Whatman) and further purified by desalting. Rotavirus particles were generously provided by Stephen Harrison's laboratory (Harvard Medical School/Howard Hughes Medical Institute). Viral RNAs were isolated using TRIzol (Sigma) and were purified by 1% (wt/vol) agarose gel electrophoresis. For fluorescein or biotin labeling of RNA, the 3′ end of RNA was oxidized with 0.1 M sodium periodate in 0.25 M NaOAc, pH 5.5, at room temperature for 2 h. The reaction subsequently was treated with 0.2 M KCl, the buffer was replaced with 0.25 M NaOAc, pH 5.5, using Zeba desalting column (Pierce), and incubation with 0.1 M fluorescein hydrazide (Life Technologies) or EZ-Link Hydrazide-PEG4-Biotin (Pierce) continued at room temperature for 4–6 h. The labeled RNA was desalted twice to remove unincorporated dye or biotin (Pierce) and was stored in 20 mM Hepes, pH 7.0, at −20 °C. The efficiency of fluorescent labeling was tested on the acrylamide gel. The efficiency of biotin labeling was examined by monitoring the mobility shift of RNA upon incubation with streptavidin.

Pull-Down Assay. For assembly kinetics, fluorescently labeled MDA5, RIG-I, or MDA5h (0.3 μM) was incubated with 3′-biotinylated dsRNA (0.6 μg/mL) at 37 °C in buffer A [20 mM Hepes (pH 7.5), 150 mM NaCl, 1.5 mM $MgCl_2$, 2 mM DTT] in the presence of 2 mM β,γ-methyleneadenosine 5′-triphosphate (ADPCP). At the indicated time points, the assembly reaction was quenched by mixing with 60 μg/mL heparin (Sigma) and 2 mM ADP·AlF_4 on ice. Before use, the heparin solution was desalted twice in buffer A. ADP·AlF_4 was prepared by mixing ADP, $AlCl_3$, and NaF in a 1:1:3 molar ratio. For measurements of dissociation kinetics, labeled MDA5, RIG-I, or MDA5h (0.6 μM) was preincubated with 3′-biotinylated dsRNA (2 μg/mL) in buffer A at 37 °C for 3 min, and the disassembly reaction was initiated by the addition of 200 μg/mL heparin and 2 mM ATP or ADPCP and was quenched at the indicated time points with 2 mM ADP·AlF_4 on ice. Quenched reactions (both assembly and disassembly) were incubated immediately with hydrophilic streptavidin magnetic beads (New England BioLabs) for 3 min on ice. Before use, the beads were preblocked with 0.5% (wt/vol) BSA in buffer A to minimize nonspecific binding. Beads were precipitated on a magnetic rack, washed three times with buffer A containing 0.05% (vol/vol) Triton X-100, and eluted by boiling at 95 °C for 2 min with 0.6% (wt/vol) SDS, 1 mg/mL heparin, 0.3 M NaCl in SDS/PAGE sample buffer before loading onto a 4–12% NuPAGE Bis-Tris SDS/PAGE gel (Life Technologies). Fluorescent gel images were recorded using a GE FLA9000 scanner.

Single-Molecule Fluorescence Assay. The single-molecule fluorescence assay was performed on the total internal reflection fluorescence (TIRF) microscopy platform as described previously (4). Briefly, the quartz slide was cleaned using piranha solution (mixture of 3:1 concentrated sulfuric acid:30% (vol/vol) hydrogen peroxide solution) and coated with a 40:1 mixture of polyethylene glycol (m-PEG-5000; Laysan Bio, Inc.) and biotinylated PEG (biotin-PEG-5000; Laysan Bio, Inc.). The flow cell was prepared by using double-sided tape (3M) between the functionalized quartz slide and glass coverslip. Polyethylene tubing (PE 50; Becton, Dickinson) was linked to the channel for successive buffer changes. To immobilize RNA, we first incubated the flow cell with T50 buffer [10 mM Tris·Cl (pH 8.0), 50 mM NaCl] containing streptavidin (0.2 mg/mL) for 2 min. The flow cell was washed with milliQ water and incubated with biotinylated RNA (~100 pM) for 2 min. Unconjugated RNA was washed out, and the flow cell was preblocked with BSA solution (20 mg/mL) for 5 min to prevent nonspecific binding of MDA5.

Single-molecule images were taken using a prism-type wide-field TIRF microscope and an electron-multiplying CCD camera (IXon DV897ECS-BV; Andor Technology) at a frame rate of 0.5–20 Hz. For experiments requiring a direct comparison of fluorescence intensities, multichanneled flow cells were used, and the laser power was kept constant by fixing the laser spot. For two-color imaging, Alexa 546 and Hylite 647 were excited with alternating lasers, and emitted light was recorded independently using dichroic mirrors. All flow cells and buffers were maintained at 37 °C during the reaction using a home-designed temperature control system manufactured by Live Cell Instrument.

For assembly reactions, fluorescently labeled MDA5, MDA5h, or $MDA5h^{SNAP}$ (50 nM) was preincubated with 2 mM ADPCP in buffer A, injected into the flow cell containing immobilized RNA (at $t = 0$), and the fluorescence signal was recorded as a function of time. The protein sample contained an oxygen scavenger system consisting of Trolox (1 mM) (Sigma), glucose oxidase (1 mg/mL) (Sigma), catalase (0.04 mg/mL) (Sigma), and glucose [0.4% (wt/vol)] (Sigma) to enhance photostability. For disassembly reactions, MDA5:dsRNA filaments were preformed in solution by mixing biotinylated RNA (0.4 nM) and MDA5 (2 μM) for 5 min at room temperature; the solution then was diluted 10-fold and injected into the flow cell for surface immobilization. Free protein and dsRNA were rinsed out with buffer A. Subsequently, buffer A containing 2 mM ATP and the oxygen scavenger system was injected into the flow cell, and the disassembly reaction was recorded as a function of time.

To monitor the slow assembly and disassembly reactions efficiently with minimal photobleaching, we used low laser power (~20-fold lower than the typical laser power used for single Alexa 647 dye detection), which increased the photobleaching

time (exponential decay time constant) from ~250 s to ~80 min. The presence of a large number of MDA5 molecules within the filaments as well as the use of longer integration times (e.g., ~2 s for the 1- to 2-kb dissociation reaction and 0.5 s for the 0.5-kb dissociation reaction) allowed reliable measurement of assembly and disassembly kinetics using the low-power laser. Comparison of the dissociation kinetics measured at various laser powers suggests that the effect of photobleaching on the dissociation kinetics is minimal (Fig. S10*A*). When monitoring fast reactions that completed within ~50 s, such as the dissociation reaction from 112-bp dsRNA, we used a higher laser power (~10–20×) and a short integration time (0.1 s) to monitor dynamics of individual molecules robustly. The step analysis of the disassembly reaction from 112-bp RNA was guided by a home-built step finding algorithm. Drift was corrected based on the image registration algorithm (5).

Prediction of Step Decrement Distributions. In analysis of the histogram of the number of stepwise decrements during disassembly of MDA5h^{SNAP} from 112-bp dsRNA in Fig. 6*F*, two models for MDA5 dissociation (monomer vs. dimer as dissociation unit) were considered under the assumption that the MDA5 binding unit is a dimer. Let p be the probability of the MDA5h^{SNAP} monomer being fluorescently labeled. Let q be the probability of the dimer being labeled (either singly or doubly). Because 112-bp dsRNA can accommodate eight MDA5 dimers, the probabilities of observation of n stepwise decrements during dissociation are $P_1(n)$ and $P_2(n)$ for monomer and dimer dissociation models, respectively. Based on the experimental measurement of Alexa 647 optical density, the labeling efficiency of MDA5h^{SNAP} was estimated as ~50% (i.e., $P = 0.5$). Predicted distribution curves in Fig. 6*F* were calculated using the following equations:

$$q = 1-(1-p)^2$$
$$P_1(n) = {}_{16}C_n \times p^n \times (1-p)^{16-n}$$
$$P_2(n) = {}_{8}C_n \times q^n \times (1-q)^{8-n}$$

1. Peisley A, et al. (2011) Cooperative assembly and dynamic disassembly of MDA5 filaments for viral dsRNA recognition. *Proc Natl Acad Sci USA* 108(52):21010–21015.
2. Antos JM, et al. (2009) Site-specific N- and C-terminal labeling of a single polypeptide using sortases of different specificity. *J Am Chem Soc* 131(31):10800–10801.
3. Sherlin LD, et al. (2001) Chemical and enzymatic synthesis of tRNAs for high-throughput crystallization. *RNA* 7(11):1671–1678.
4. Roy R, Hohng S, Ha T (2008) A practical guide to single-molecule FRET. *Nat Methods* 5 (6):507–516.
5. Guizar-Sicairos M, Thurman ST, Fienup JR (2008) Efficient subpixel image registration algorithms. *Opt Lett* 33(2):156–158.

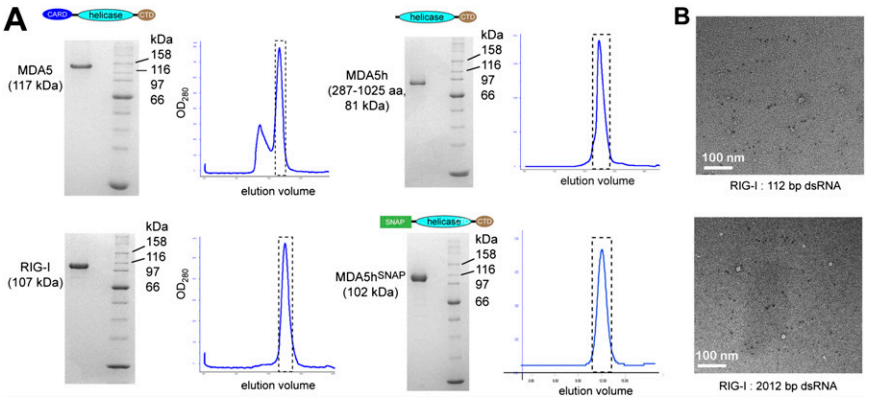

Fig. S1. Purification of recombinant proteins. (*A*) Coomassie blue-stained SDS/PAGE gels and SEC chromatograms of full-length MDA5 and RIG-I, CARD truncation mutant (MDA5h), and MDA5h fused to SNAP (MDA5h^{SNAP}). SEC was performed using a GE Superdex 200 10/300 column. The predicted masses of the proteins are shown in parentheses. (*B*) Representative electron micrographs of RIG-I (100 nM) in complex with 112-bp or 2,012-bp dsRNA (2.4 μg/mL) in the presence of 0.5 mM ADP·AlF$_4$.

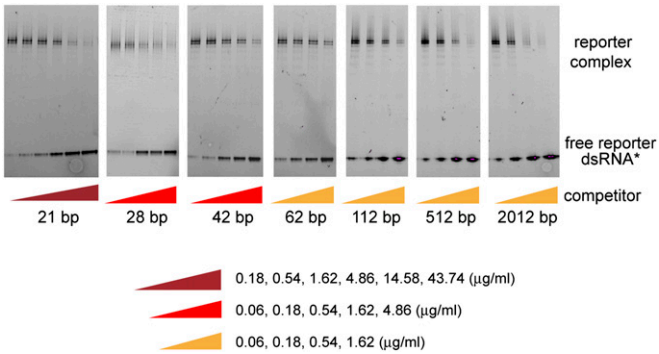

Fig. S2. Competition binding assay of MDA5, Native PAGE images of the competition binding assay shown in Fig. 1*D*. Fluorescein-labeled 112-bp dsRNA (dsRNA*) (0.6 μg/mL) and unlabeled competitor dsRNAs (21- to 2,012-bp dsRNAs) were coincubated with MDA5. Disappearance of the labeled complex was monitored by EMSA in the presence of increasing amounts of competitor dsRNAs.

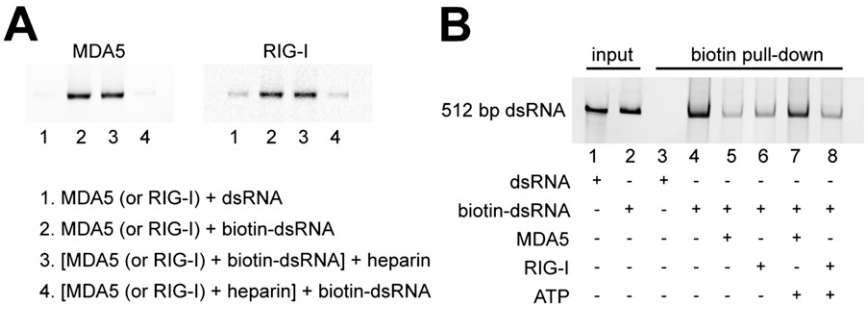

Fig. S3. Biotin pull-down assays. (*A*) Labeled MDA5 and RIG-I (0.3 μM) were preincubated with 3′-biotinylated 512-bp dsRNA (0.6 μg/mL) or heparin (60 μg/mL) at 37 °C for 5 min and subsequently were incubated with heparin (60 μg/mL) or 3′-biotinylated 512-bp dsRNA (0.6 μg/mL), respectively, at 37 °C for an additional 5 min. The pull-down results indicate that heparin does not induce dissociation of MDA5 and RIG-I from dsRNA but is able to sequester MDA5/RIG-I released from dsRNA. Similar results were obtained with 1.2 or 2 μg/mL of dsRNA in combination with heparin in 100-fold excess of dsRNA. (*B*) The recovery efficiency of dsRNA using streptavidin pull-down was analyzed using TBE-PAGE stained with SybrGold (Life Technologies). 3′-Biotinylated 512-bp dsRNA (0.6 μg/mL) was incubated with MDA5 or RIG-I and subjected to pull-down. The level of recovery of RNA without a biotin tag was below the detection limit, suggesting that pull-down is specific for biotinylated dsRNA. Binding of MDA5 or RIG-I (0.3 μM) reduces the recovery efficiency of dsRNA to ~30% of that without MDA5/RIG-I, probably because of steric occlusion of the biotin tag by MDA5/RIG-I. Because rates were calculated using relative values normalized against the saturation level, the reduced recovery efficiency should not affect the interpretation of RNA binding and dissociation kinetics. In addition, results from the biotin pull-down assays are in concordance with the results from single-molecule studies and other bulk analyses such as ATP hydrolysis lag phase and single-round kinetics.

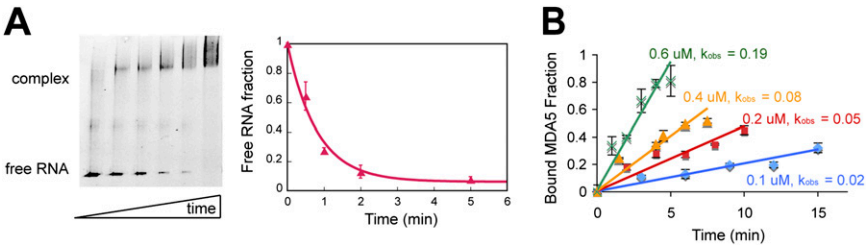

Fig. S4. MDA5 binds to dsRNA with slow kinetics. (*A*) Analysis of RNA binding kinetics of MDA5 using time-dependent EMSA. MDA5 (0.3 μM) was incubated with 3′-fluorescein–labeled 512-bp dsRNA (0.6 μg/mL) for the indicated time periods, and the reaction was quenched on ice with heparin in 100-fold excess of RNA before gel analysis. On the right is the quantitative analysis of the level of free dsRNA during the binding reaction and a fitted single exponential curve (mean ± SD; $n = 3$). (*B*) Analysis of RNA binding kinetics of MDA5 using biotin pull-down kinetic assays. Experiments were performed as in Fig. 4*A*. The apparent binding rates (k_{obs}s) were derived from linear fits and were plotted against the MDA5 concentration in Fig. 4*B* to calculate the binding rate constant, k_{on}.

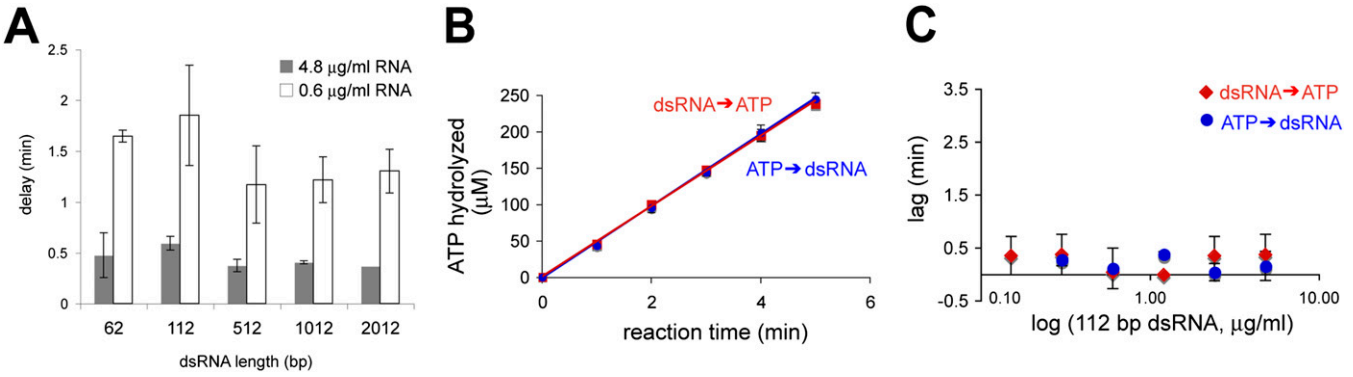

Fig. S5. The ATP hydrolysis reaction of MDA5, but not RIG-I, initiates after a delay. (*A*) The lag phase of ATP hydrolysis reaction of MDA5 (0.3 μM) with 62- to 2,012-bp dsRNAs (4.8 or 0.6 μg/mL) (mean ± SD, *n* = 3). (*B*) Time evolution of the ATP hydrolysis reactions of RIG-I (mean ± SD, *n* = 3). The reaction was initiated by the addition of ATP to a preformed complex of RIG-I (30 nM) and 112-bp dsRNA (0.6 μg/mL) (dsRNA→ATP) or by the addition of dsRNA to a preformed complex of RIG-I and ATP (ATP→dsRNA). (*C*) The lag phase of RIG-I using 112-bp dsRNA at various concentrations (mean ± SD, *n* = 3). Reactions were performed as in *B*.

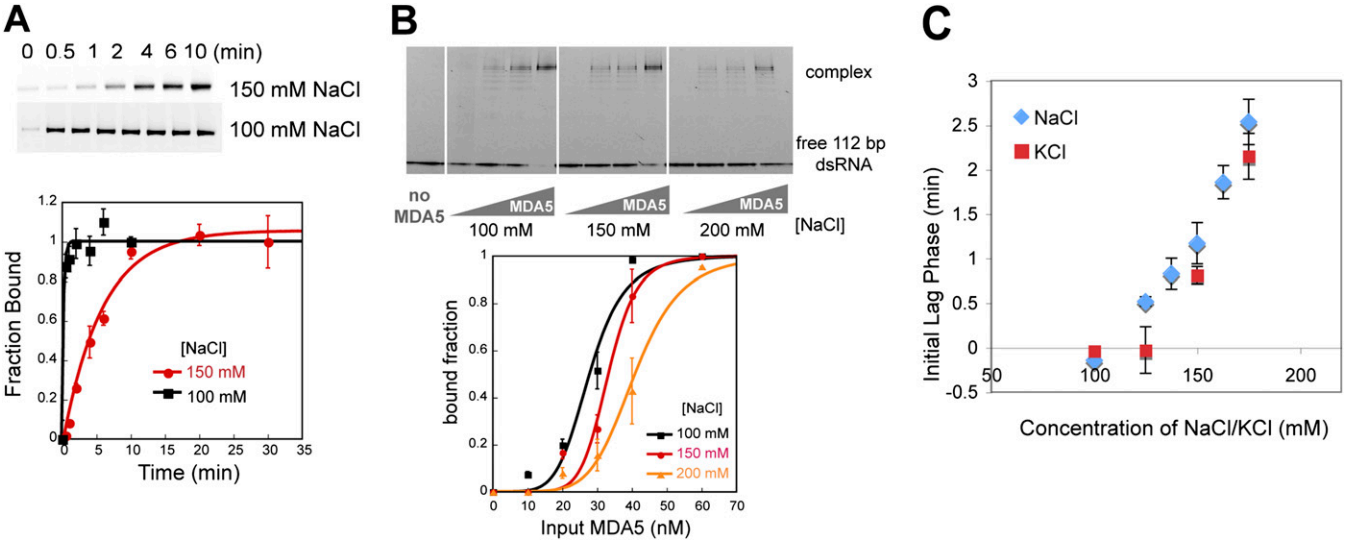

Fig. S6. Low ionic strength promotes MDA5 binding to dsRNA. (*A*) Comparison of 512-bp dsRNA binding kinetics of MDA5 in buffer containing 150 vs. 100 mM NaCl. The biotin pull-down assay was performed as in Fig. 4*A*. Shown below is the quantitation of the bound fraction as a function of time (mean ± SD, *n* = 4). (*B*) EMSA of MDA5 titration with 3′ fluorescein-labeled 112-bp dsRNA (3 nM) incubated in binding buffers containing 100, 150, and 200 mM NaCl for 15 min at 37 °C. MDA5 concentrations used for titration were 25, 50, 100, and 200 nM. Shown below is the quantitation of the bound fraction as a function of MDA5 concentration (mean ± SD, *n* = 3). (*C*) Initial lag phase in the ATP hydrolysis reaction of MDA5 in buffers containing 100–175 mM NaCl or KCl (mean ± SD, *n* = 2–4).

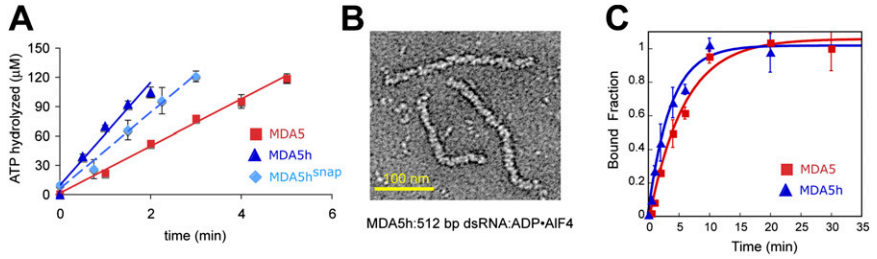

Fig. S7. Comparison of biochemical properties of MDA5 and MDA5h. (*A*) Time evolution of the ATP hydrolysis reactions of MDA5, MDA5h, and MDA5h^{SNAP} (0.3 μM) using 112-bp dsRNA (4.8 μg/mL) (mean ± SD, *n* = 3). MDA5 was preincubated with dsRNA, and the reaction was initiated by the addition of ATP to the MDA5:dsRNA complex. (*B*) Representative electron micrograph of MDA5h filament formed with 512-bp dsRNA. (*C*) Time evolution of the dsRNA-bound fraction of MDA5 or MDA5h as measured by the pull-down kinetic assay (mean ± SD, *n* = 3). Experiments were performed as in Fig. 4*A*.

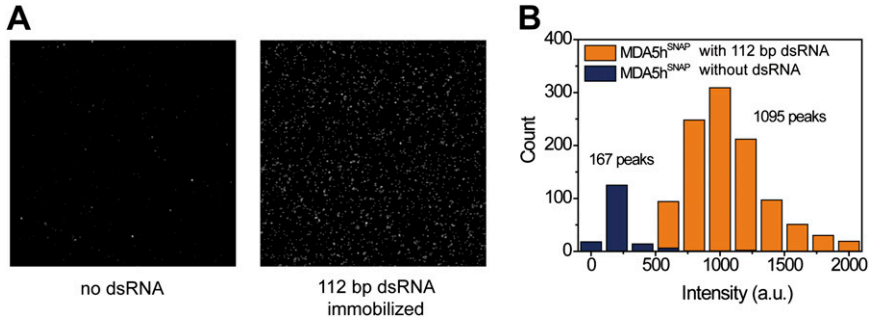

Fig. S8. Comparison of dsRNA-dependent and -independent binding of MDA5 to the flow cell surface. (*A*) Representative fluorescence images of MDA5h^{SNAP} bound to flow cells. Alexa 647-labeled MDA5h^{SNAP} (200 nM) was injected into the flow cell with or without immobilized 112-bp dsRNA, and unbound MDA5h^{SNAP} was washed out before fluorescence imaging. (*B*) Intensity distribution of the MDA5h^{SNAP} fluorescence signal observed in *A*. Both the frequency and the fluorescence intensity of MDA5h^{SNAP} particles are significantly higher in the dsRNA-coated flow cell than in the empty one [mean = 1,100 arbitrary units (a.u.) vs. 210 a.u].

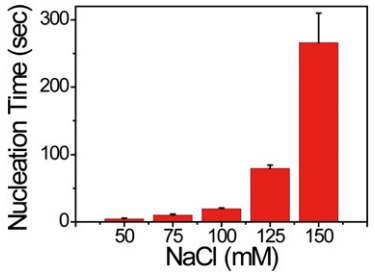

Fig. S9. Salt concentration dependence of the nucleation time of filament formation by MDA5h^{SNAP}. Nucleation time was measured on the surface-immobilized 512-bp dsRNA using 50 nM MDA5h^{SNAP} as in Fig. 5*H*. *n* = 760–2,095 for each sample.

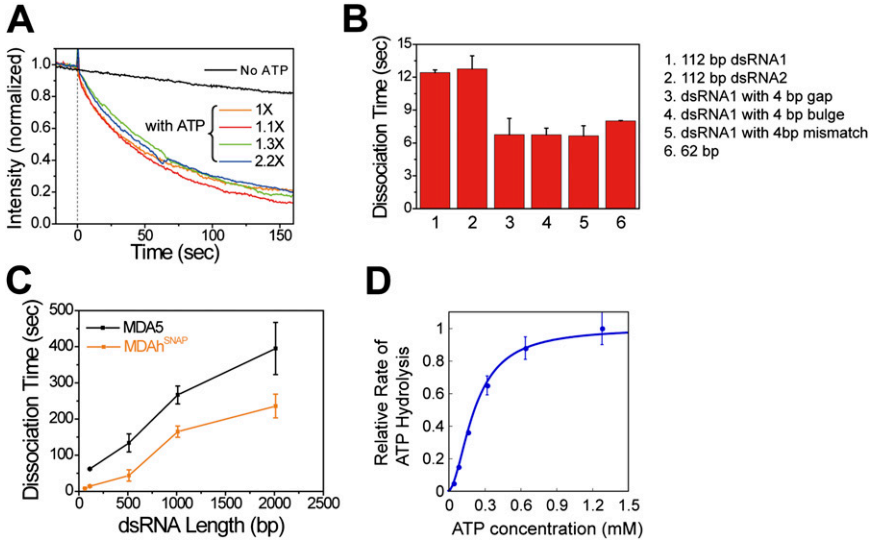

Fig. S10. Single-molecule measurement of dissociation kinetics of MDA5h^{SNAP} filaments. (*A*) Averaged traces of disassembly reaction of MDA5h^{SNAP} filaments formed on 512-bp dsRNA. Disassembly traces were recorded at various laser powers (1–2.2×). *n* = ~500–700 for each sample. (*B*) Dissociation time constants of MDA5h^{SNAP} using dsRNAs with or without structural irregularities (as defined in Fig. 2*C*). *n* = ~300–600. (*C*) Dissociation time constants of MDA5 and MDA5h^{SNAP} using 512-, 1,012-, and 2,012-bp dsRNAs (*n* = ~400–700). (*D*) Dependence of ATP hydrolysis rate on ATP concentration. ATP hydrolysis rate of MDA5 (0.3 μM) with 512-bp dsRNA (3.6 μg/mL) at varying concentrations of ATP is shown (mean ± SD, *n* = 2). Rates are normalized against the rate at 1.2 mM ATP.

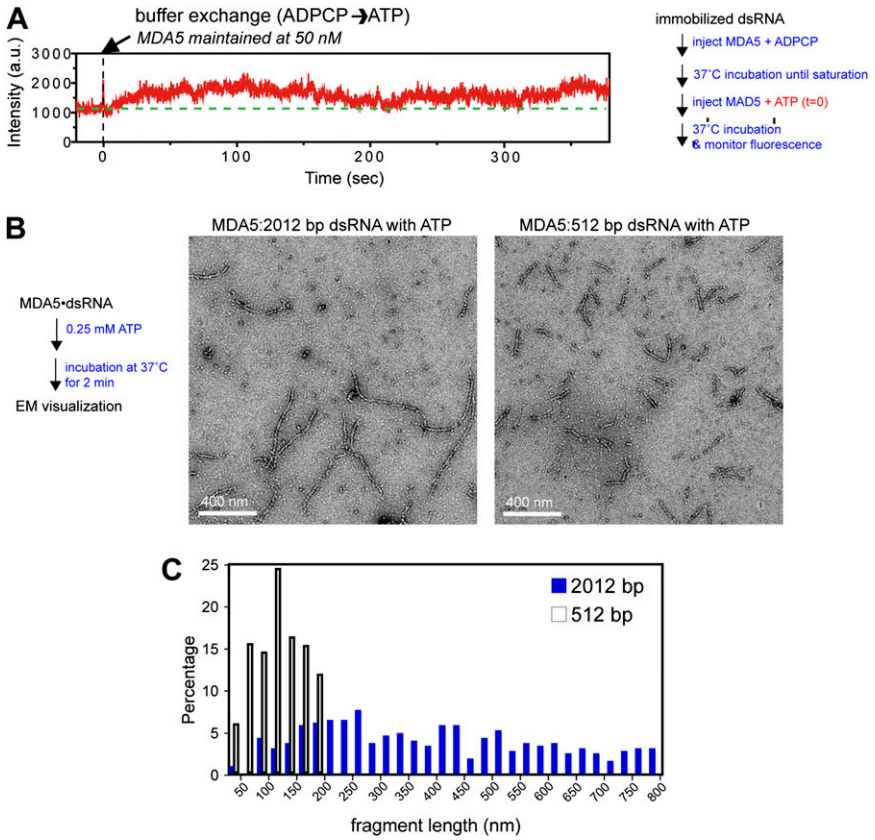

Fig. S11. Dynamics of MDA5 filaments during ATP hydrolysis. (*A*) A representative trace of an MDA5h^{SNAP} filament before and after buffer change (at $t = 0$) from ADPCP to ATP. We first incubated surface-immobilized 2,012-bp dsRNA with MDA5h^{SNAP} (200 nM) and ADPCP (2 mM) until the fluorescence intensity reached a plateau and then replaced the buffer with buffer containing MDA5h^{SNAP} (200 nM) and ATP (0.5 mM). The green dotted line indicates the saturation level of the filament assembled in the presence of ADPCP. Upon ATP injection, the fluorescence intensity displayed strong fluctuation, indicating repetitive cycles of assembly and disassembly processes. However, the average intensity was ~50% higher with ATP than with ADPCP, consistent with the notion that concurrent actions of disassembly and assembly repair filament discontinuity. (*B*) Representative electron micrographs of MDA5 with 2,012- and 512-bp dsRNA during the ATP hydrolysis steady state. The preformed complex of MDA5 (0.3 μM) and dsRNA (1.2 μg/mL) was incubated with 0.25 mM ATP for 2 min at 37 °C and was visualized directly by electron microscopy without incubation with ADP·AlF_4 or heparin. (*C*) Histogram of filament lengths during the ATP hydrolysis steady state ($n = 400$ each).

Table S1. Sequences of the in vitro transcribed RNAs used in this study

21-bp dsRNA	aggucacgacguuguaaaccu
28-bp dsRNA	The first 16 bp of the MDA5 gene flanked by 5′-gggaga and tcttcc-3′
42-bp dsRNA	The first 30 bp of the MDA5 gene flanked by 5′-gggaga and tctccc-3′
62-bp dsRNA	The first 50 bp of the MDA5 gene flanked by 5′-gggaga and tctccc-3′
112-bp dsRNA1	The first 100 bp of the MDA5 gene flanked by 5′−gggaga and tctccc-3′
112-bp dsRNA2	The first 100 bp of the T7 RNA polymerase gene flanked by 5′-gggaga and tctccc-3′
162-bp dsRNA	The first 150 bp of the MDA5 gene flanked by 5′-gggaga and tctccc-3′
512-bp dsRNA	The first 500 bp of the MDA5 gene flanked by 5′-gggaga and tctccc-3′
1,012-bp dsRNA	The first 1,000 bp of the T7 RNA polymerase gene flanked by 5′-gggaga and tctccc-3′
2,012-bp dsRNA	The first 2,000 bp of the T7 RNA polymerase gene flanked by 5′-gggaga and tctccc-3′

All dsRNAs contain a 5′-triphosphate group at each end unless otherwise stated.